ISSN 0020-4412, Instruments and Experimental Techniques, 2024, Vol. 67, No. 5, pp. 911–918. © Pleiades Publishing, Ltd., 2024.

ELECTRONICS AND RADIO ENGINEERING

Four-Photon Josephson Traveling Wave Parametric Amplifier

A. A. Lomonosov[a], R. V. Kubrakov[a], L. V. Filippenko[a], R. K. Kozulin[a], V. A. Krupenin[b], V. K. Kornev[b], and M. A. Tarasov[a,*]

[a] *Kotelnikov Institute of Radio Engineering and Electronics, Russian Academy of Sciences, Moscow, 125009 Russia*

[b] *Moscow State University, Moscow, 119991 Russia*

**e-mail: tarasov@hitech.cplire.ru*

Received August 27, 2024; revised September 6, 2024; accepted September 11, 2024

Abstract—Josephson traveling wave parametric amplifiers can have ~~a wide gain~~ frequency range, high sensitivity, and low noise, which makes them promising for quantum computing, array receiver readout systems, spectroscopy, single-photon detectors, etc. In this paper, the authors investigate samples of traveling wave parametric amplifiers based on a three-layer Nb/AlO_x/Nb superconductor-insulator-superconductor (SIS) structure with a ~~single~~ SNAIL (Superconducting Nonlinear Asymmetric Inductive eLements) ~~cell~~ consisting of the kinetic inductance of four SIS junctions and the nonlinear inductance of a smaller SIS junction. The cells are alternately connected in antiphase with respect to the magnetic flux, which ensures a change in the sign of the Kerr nonlinearity and a reduction in the phase mismatch for the pump frequency, signal frequency, and ~~mirror~~ frequency. The transmission spectra of the samples were measured at temperatures of 4.2 K and 2.8 K in the frequency range of 0.1–6 GHz.

DOI: 10.1134/S0020441224701586

1. INTRODUCTION

In a parametric amplifier, a powerful pump wave at a frequency is fed to the input ~~f_P~~ together with a weak amplified signal f_S. The electric current of the pump wave modulates the nonlinear reactance and, by mixing frequencies, produces an amplification of the signal at the frequency f_S as well as the generation of ~~a mirror~~ signal at a frequency f_I. The theory of such amplifiers was created in [1]. In our case, an amplifier with pumping of the nonlinear inductance of the Josephson junction (JJ) superconductor–insulator–superconductor (SIS junction, Fig. 1) is implemented in a long coplanar line. The impedance of such an infinite line without losses is

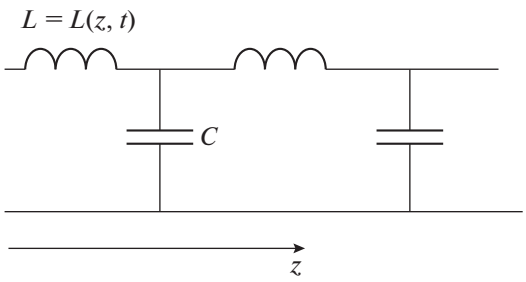

Fig. 1. Transmission line with nonlinear inductance.

$$Z_0 = \frac{i\omega L}{2} + \sqrt{\frac{L}{C} - \frac{\omega^2 L^2}{4}},$$

or

$$Z_0 = \rho_0 \left(\sqrt{1 - \left(\frac{\omega}{\omega_{cp}} \right)^2} + i \frac{\omega}{\omega_{cp}} \right),$$

where the wave resistance

$$\rho_0 = \sqrt{\frac{L}{C}},$$

and cutoff frequency

$$\omega_{cp} = \frac{2}{\sqrt{LC}},$$

while $|Z_0| = \rho_0$ and $\omega \le \omega_{cp}$. It is clear that the impedance of such a line is always complex and it is impossible to completely match the impedances of a Josephson traveling wave parametric amplifier (JTWPA) and the actual impedance of a transmission line with a resistance of 50 Ohms over the entire frequency range (Fig. 2).

The power ratios of the pump wave, signal wave, and ~~mirror~~ wave satisfy the Manley–Rowe equations. They represent energy relationships for the interaction of several oscillations in nonlinear systems. For a para-

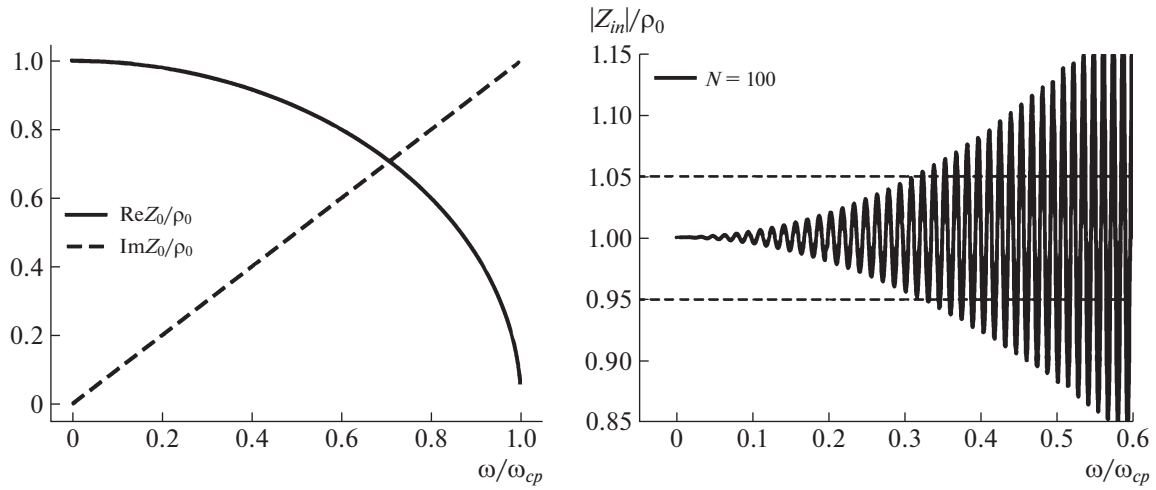

Fig. 2. Real and imaginary parts of the impedance of a continuous line using a simple formula and calculation of the impedance mismatch of a discrete line with a real load [2].

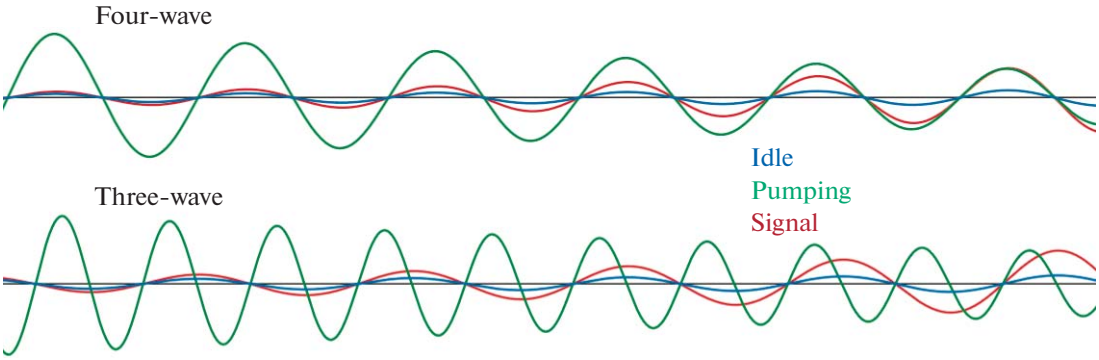

Fig. 3. Schematic representation of amplification in two modes: four-wave and three-wave.

metric amplifier at the pump frequency f_p, signal frequency f_s, and mirror (~~idle~~) frequency f_i, they look like

$$\frac{P_p}{f_p} = \frac{P_s}{f_s} = \frac{P_i}{f_i},$$

i.e., the power from the pump source is redistributed in the simplest case between two oscillations. To amplify the signal, there must be another wave in the line: an ~~idle~~ or mirror wave $f_I = f_P - f_S$. In this case, there are two possible signal amplification schemes for nonlinear elements: three-photon and four-photon (Fig. 3).

Depending on the type of nonlinearity used, it is possible to implement a four-photon mixing process, where the relationship between frequencies has the form

$$2f_P = f_S + f_I, \quad (1)$$

or the three-photon mixing process, where the relationship is

$$f_P = f_S + f_I. \quad (2)$$

Ratios (1) and (2) represent the law of conservation of energy of photons participating in the mixing process. The law of conservation of momentum requires a similar relationship for wave vectors k: in four-photon mixing mode

$$2k_P = k_S + k_I, \quad (3)$$

in three-wave mixing mode

$$k_P = k_S + k_I. \quad (4)$$

Ratios (3) and (4) are also known as phase-matching conditions and are necessary to amplify the signal. It should be emphasized that the generation of a mirror frequency signal f_I and the power of the amplified signal f_S are linearly related, which follows from the conditions (1)–(4). Therefore, the suppression of the mirror frequency f_I will result in signal gain suppression f_S.

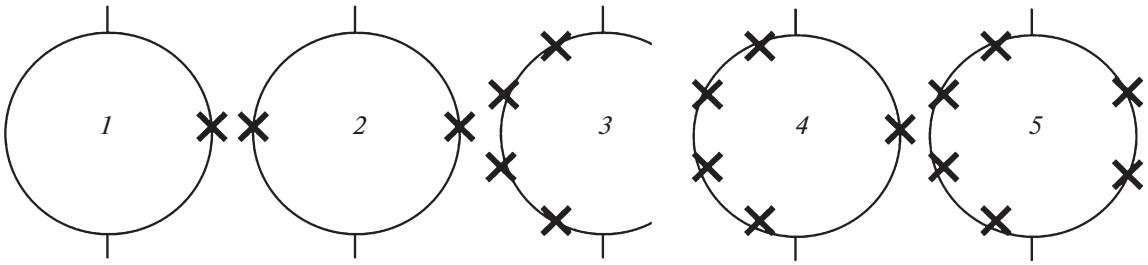

Fig. 4. Cells in the form of (*1*) RF SQUID, (*2*) ~~PT~~ SQUID, (*3*) kinetic inductance of four JJ, (*4*) SNAIL structures in the form of a SQUID with a loop of kinetic inductance of four large JJs and one small nonlinear JJ and (*5*) the same with two small JJ.

The propagation of a voltage wave in a line can be described by the formula

$$V_n(t) = V_0 \exp[i(\omega t - kx_n)],$$

where $k = 2\pi/\lambda = \omega/v$ is wave number and $x_n = an$ is coordinate of the nth cell. It is also necessary to keep in mind that the phase velocity decreases with frequency from

$$v_{\text{~~@English~~ term@}}(\omega = 0) = \frac{a\omega_{\text{cp}}}{2} = \frac{a}{\sqrt{LC}},$$

up to 0.65 at line cutoff frequency ω_{cp}. In both modes, energy from the pump wave is first transferred to the mirror (idle) wave, then back to the signal wave, and parametric amplification of the signal occurs. In the three-photon mode, one pump photon is converted into a signal photon and a mirror photon. In the four-photon mode, two pump photons are converted into a signal photon and a mirror photon. It should be emphasized that the generation of a mirror frequency signal f_I and the power of the amplified signal f_S are linearly related, which follows from the law of conservation of energy in the form of Manley–Rowe relations

$$\frac{P_p}{f_p} = \frac{P_s}{f_s} = \frac{P_I}{f_I}.$$

Therefore, the suppression of the mirror frequency f_I will result in signal gain suppression f_S.

2. SINGLE CELL AND CHAIN

The studied JTWPAs consist of ~~single~~ cells in the form of superconducting quantum interference devices, SQUIDs. Let us consider several variants of SQUIDs since they are used in different variants of parametric amplifier cell design (Fig. 4): RF SQUID with one JJ and an inductive loop, DC SQUID (direct current SQUID) with two JJs and an inductive loop, kinetic inductance from four JJs, RF SQUID with kinetic inductance and one small JJ, RF SQUID with kinetic inductance of the loop and two JJs to increase nonlinearity.

SNAIL (Superconducting Nonlinear Asymmetric Inductive eLements) type JTWPA samples have been developed and manufactured. The cell consists of four ~~transitions~~ on one side of the ring and two ~~transitions~~ with different parameters on the other side of the ring (Fig. 5). In fact, this design is an RF SQUID with kinetic inductance (four junctions on the left) and a composite Josephson junction on the right (Fig. 6).

Large SIS junctions with an area of 20 μm^2 and small ~~transitions~~ of with an area of 5 μm^2 should have had resistances of approximately 100 Ohm and 400 Ohm according to calculations, critical currents should be 16 and 4 μA according to the Ambegaokar–Baratov theory, and Josephson inductances should be 20 and 80 pH. Geometric inductance of a loop with an area of 300 μm^2 was estimated ~~at~~ 25 ~~pGy~~. The total loop inductance, including the geometric inductance and the inductance of the four JJs, is 150 pH. Capacitors to ground with an area of 250~~2~~ ~~microns~~ are rated for 45 fF capacitance. The impedance of a coplanar line with such elements is estimated to be 60 Ohms. The line cutoff frequency will be 60 GHz, while the plasma frequency with a loop capacitance of 0.5 pF will be 20 GHz. Inductive parameter by calculation $\beta_L = L_{\text{loop}}/2L_{\text{junc}} = 150/160 = 0.93$, which is actually less.

Each subsequent cell is symmetrically ~~rotated~~ relative to the axis, due to which the parametric amplifier mode with a variable sign Kerr effect is realized. For the first time, such a mode for phase matching in a four-wave JTWPA was proposed in theoretical work [3]. Practical implementation in [4] made it possible to achieve phase matching of 6 and 10 GHz with pumping at 8 GHz and a gain of more than 20 dB. The alternating polarity of the magnetic flux in adjacent cells suppresses the undesirable three-photon amplification process and allows for an optimal four-photon process. Due to the alternating sign of the Kerr phase modulation, the total phase mismatch is reduced. The advantage of this configuration is the ability to change the pump frequency over a wide range, in contrast to a circuit with resonant elements to achieve phase matching, in which the pump frequency is fixed.

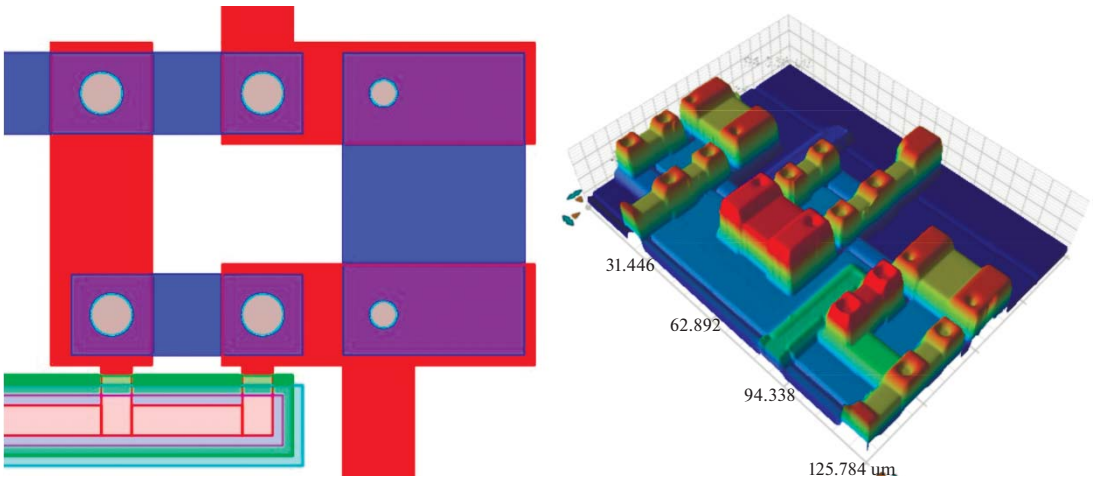

Fig. 5. On the left is a schematic image of a SNAIL type JTWPA cell (superconducting ~~levels~~ are indicated in red and blue, Josephson junctions are in gray circles); on the right is a real image of a fragment of the manufactured circuit in an optical profilometer.

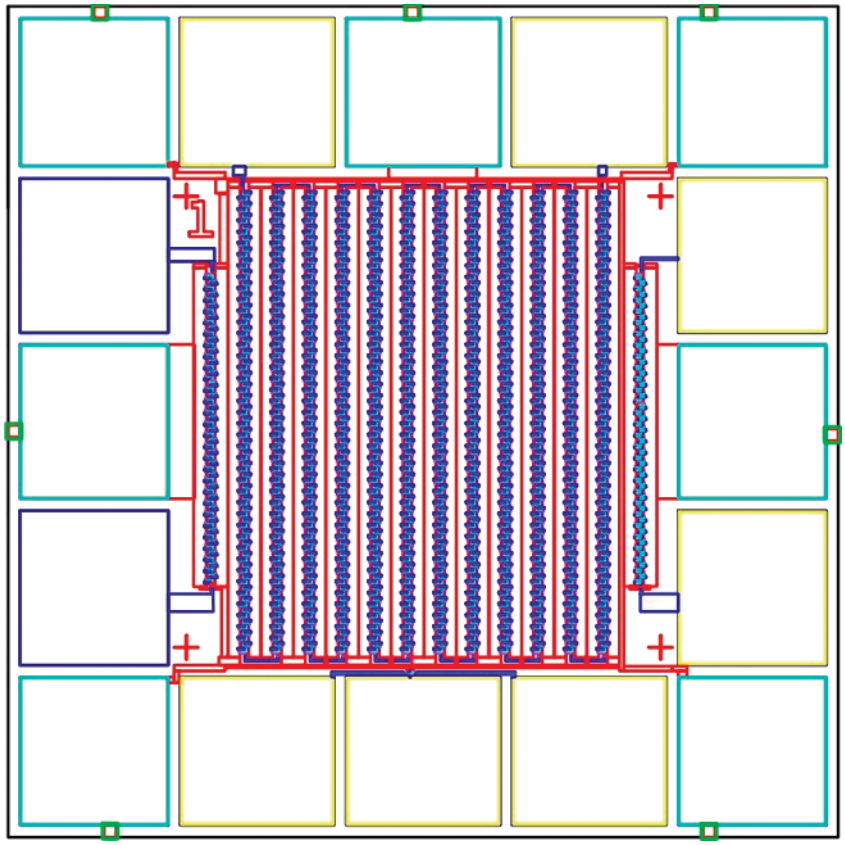

Fig. 6. Design of the JTWPA chip.

The chip is 7×7 mm^2 in size. It consists of 16 contact pads, between which there are chains of cells of different lengths: there are short lines of 50 cells each on the right and left, and there is a long line with 1000 cells in the middle. In addition, a single SQUID is located at the bottom of the chip to allow its separate measurement. Thus, each chip contains more than 6000 ~~transitions.~~

In our earlier work [5], we investigated samples of JTWPA with ~~transitions~~ based on the Al/AlO$_x$/Al

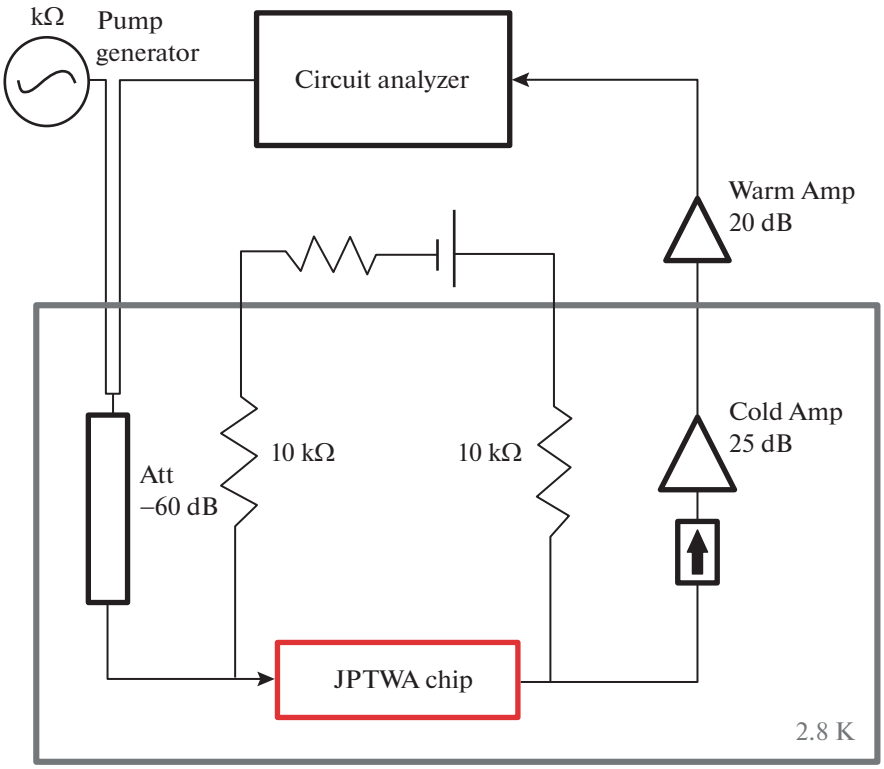

Fig. 7. Schematic diagram of the measurement in a Gifford–McMahon cryostat.

structure. One of the most important parameters in choosing a material for the manufacture of JTWPA is the critical temperature: it is 1.18 K for aluminum. If we take niobium as a material for ~~transitions,~~ it should be taken into account that its critical temperature is 9.2 K, which means that it will be sufficient to use liquid helium to achieve the required operating temperatures. Therefore, a three-layer niobium structure Nb/AlO_x/Nb was chosen as the material for the parametric amplifier ~~transitions.~~

All laboratory-made samples were previously measured in a Dewar transport vessel at liquid helium temperature (4.2 K) using a cryoprobe; the most suitable chips were selected from them for measurement in a Gifford–McMahon cryostat at 2.8 K. The cryoprobe is a tube with a sample holder at one end; it is equipped with a magnetic shield to prevent external interference and improve measurement accuracy. The basic diagram of the cryostat installation is shown in Fig. 7, and a photo of the cold stage installation is in Fig. 8.

3. SCHEME OF MEASURING INSTALLATION IN CRYOSTAT

The transmission spectra of the chip are recorded using the domestic Arinst VNA-PR1 vector network analyzer. The HP8684B was used as a pump generator. The signal goes into the cryostat via coaxial cables, and it mixes with the pump wave via a ~~tee;~~ then the waves go through a cold attenuator with a total attenuation of 60 dB into the amplifier chip; after the waves pass through the amplifier cell chain, the result of their interaction goes into the ~~valve~~ and then into the cold semiconductor amplifier (with a gain of 25 dB in the frequency range of 2–6 GHz); after leaving the cold section, the signal goes into the warm amplifier (with a gain of 20 dB up to 6 GHz) and returns to the network analyzer. The chip is also connected via resistors (10 kOhm on each side) to the DC bias and ~~gain connector~~; this allows one to set the DC bias and take I–V curves. A carbon thermometer is also located on the cold ~~heel~~ of the setup to measure the actual temperature of the sample holder.

Limitations on the measured spectrum are introduced by two elements of the setup. First, the network analyzer measures frequencies from 500 to 6000 MHz; second, the isolator installed before the cold amplifier has low bandwidth at frequencies below 2000 MHz. Therefore, the final characteristics of the samples are limited to the range of 2–6 GHz, with the pump frequency set by the generator (6.1 GHz).

Using a cryoprobe, the I–V characteristics of the samples were recorded (Fig. 9), and those most appropriate to the requirements of the experiment were selected. For the best manufactured structures, the resistance of the JTWPA line at room temperature exceeds 600 kOhm for long (1000 elements) and 30 kOhm for short (50 elements) chains, the resistance

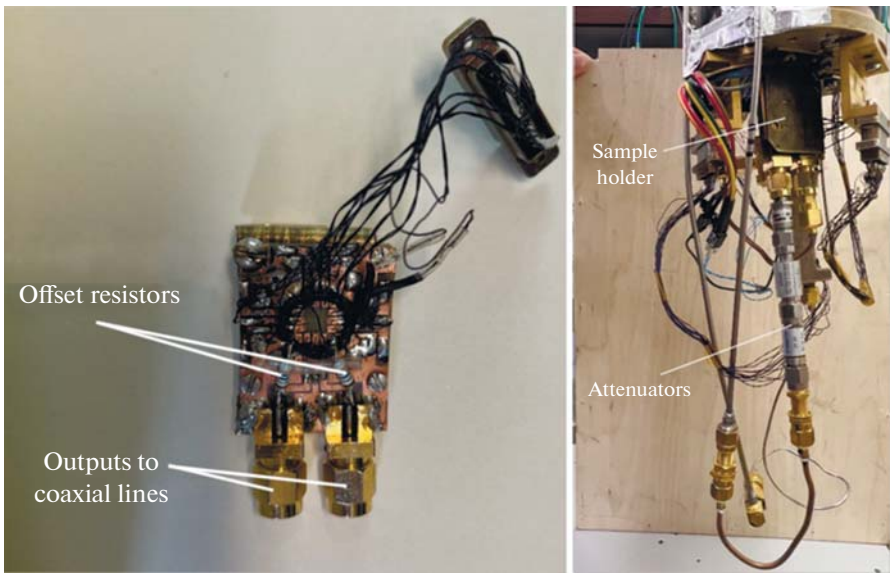

Fig. 8. Sample holder on the left and cold plate on the right.

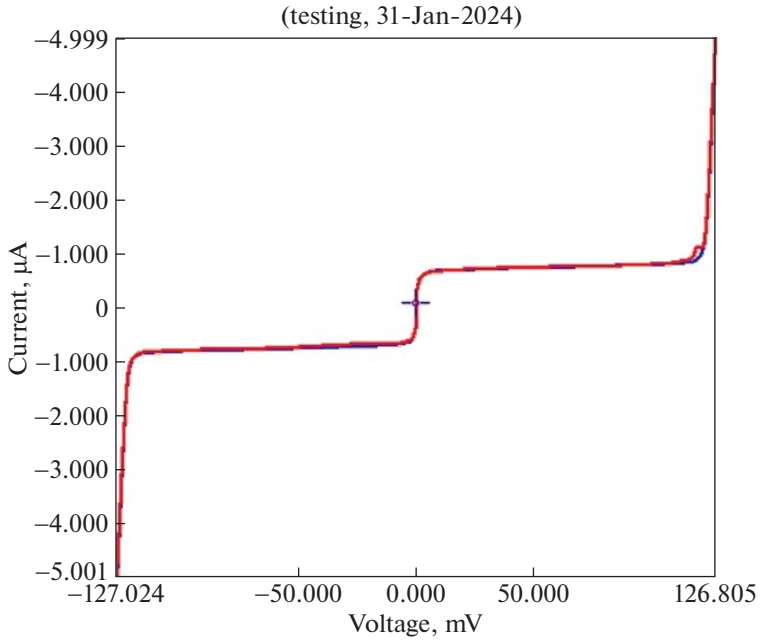

Fig. 9. ~~Volt–ampere characteristic~~ of a short chain of 50 SNAIL cells, calculated total gap 2.8 × 4 × 100 = 112 mV, measured critical current 1 μA.

to ground exceeds 2 MOhm, which means the absence of both breaks and short circuits to the common electrode. The selected sample with SNAIL design was placed in a closed-cycle Gifford–McMahon cryostat setup. Its transmission spectrum was studied in the absence of a pump signal and with a pump of 6.1 GHz (Fig. 10) as well as the approximation of this dependence by cubic piecewise smooth functions (Fig. 11). The jagged spectral response is typical for lumped element devices. The sample chain contains more than 6000 ~~transitions,~~ and the transmission spectrum is strongly frequency dependent with such a large number of ~~nonlinearities.~~

To make the result more visual, we performed two variants of data processing: approximating smoothing of the characteristics and subtraction of the transmission coefficients with and without pumping. The sample showed nonuniform gain in the 2–6 GHz band. Moreover, in the range from 5 to 6 GHz, the gain

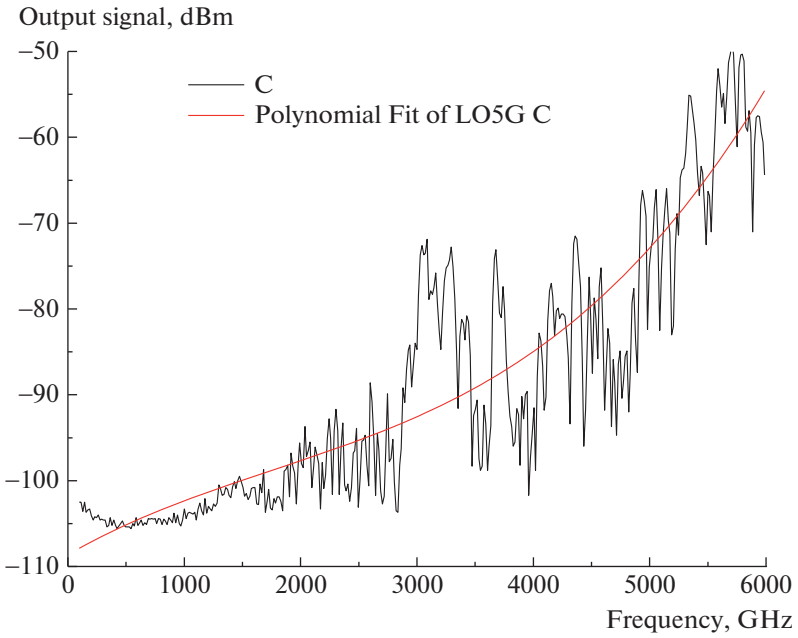

Fig. 10. Spectrum at the output of a sample with a pump signal of 6.1 GHz.

reaches 25 dB. This design contains various inhomogeneities in the ~~sample~~ path and holder, which leads to the appearance of multiple reflections.

4. CONCLUSIONS

The design has been developed and samples of the JTWPA with a cell in the form of a superconducting nonlinear asymmetric inductive element (SNAIL) have been manufactured. On a chain of 1000 elements, the maximum gain reaches 20 dB. The rather high nonuniformity of spectral transmission up to 20 dB is explained by the mismatch of impedances at the input and output since it is impossible to achieve matching of the purely active resistance of 50 Ohm at the input and output with the fundamentally complex ~~resistance~~ of an artificial transmission line in the form of a chain of purely reactive lumped elements at all frequencies. It is important to note that, under the action of pumping, the inductance is modulated, which inevitably causes variations in the reflection coefficient and gain. This problem can be solved by using a balanced amplifier with two phase-shifted gain channels. In addition, each cell and turn of the coplanar line represents a ~~heterogeneity~~, from which the reflection of propagating waves also occurs.

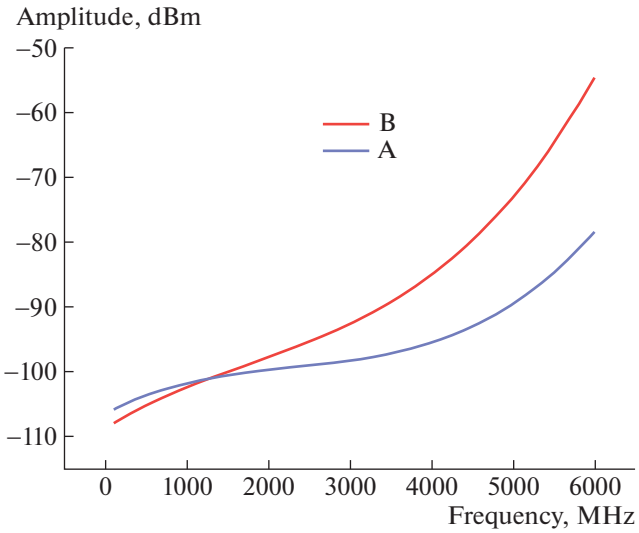

Fig. 11. Approximation of the transmission spectra of the JTWPA (a) with and (b) without 6.1 GHz pumping turned on.

FUNDING

This work was supported by ~~ongoing institutional funding. No additional grants to carry out or direct this particular research were obtained~~.

CONFLICT OF INTEREST

The authors of this work declare that they have no conflicts of interest.

REFERENCES

1. Cullen, A.L., *Proc. IEE – Part B: Electron. Commun. Eng.*, 1960, vol. 107, no. 32, p. 101. https://doi.org/10.1049/pi-b-2.1960.0085.

2. Nikolaeva, A.N., Kornev, V.K., and Kolotinsiy, N.V., *MDPI Appl. Sci.,* 2023, vol. 13, p. 8236. https://doi.org/10.3390/app13148236
3. Bell, M.T. and Samolov, A., *Phys. Rev. Appl.,* 2015, vol. 4, p. 024014. https://doi.org/10.1103/PhysRevApplied.4.024014
4. Randavie, A., Esposito, M., Planat, L., Bonet, E., Naud, C., Buisson, O., Guichard, W., and Roch, N., *Nat. Commun.,* 2022, vol. 13, p. 737. https://doi.org/10.1038/s41467-022-29375-5
5. Tarasov, M., Gunbina, A., Lemzyakov, S., Nagirnaya, D., Fominskii, M., Chekushkin, A., Koshelets, V., and Goldobin, E., ~~*Fiz. Tverd. Tela,* 2021, vol. 65, no. 9, p. 1223~~.

SPELL; OK